A Journal of the Gesellschaft Deutscher Chemiker
Angewandte
GDCh
International Edition
Chemie
www.angewandte.org

Accepted Article

Title: Reshaping the Cathodic Catalyst Layer for Anion Exchange Membrane Fuel Cells: from Heterogeneous Catalysis to Homogeneous Catalysis

Authors: Rong Ren, Xiaojiang Wang, Hengquan Chen, Hamish Andrew Miller, Ihtasham Salam, John Robert Varcoe, Liang Wu, Youhu Chen, Hong-Gang Liao, Ershuai Liu, Francesco Bartoli, Francesco Vizza, Qingying Jia, and Qinggang He

To be cited as: *Angew. Chem. Int. Ed.* 10.1002/anie.202012547

Link to VoR: https://doi.org/10.1002/anie.202012547

WILEY-VCH

10.1002/anie.202012547

WILEY-VCH

Reshaping the Cathodic Catalyst Layer for Anion Exchange Membrane Fuel Cells: from Heterogeneous Catalysis to Homogeneous Catalysis

Rong Ren,[a] Xiaojiang Wang,[a] Hengquan Chen,[a] Hamish Andrew Miller,*[b] Ihtasham Salam,[c] John Robert Varcoe,[c] Liang Wu,*[d] Youhu Chen,[e] Hong-Gang Liao,[e] Ershuai Liu,[f] Francesco Bartoli,[b] Francesco Vizza,[b] Qingying Jia,[f] and Qinggang He*[a,g]

[a] Dr. R. Ren, X. Wang, Dr. H. Chen, Dr. Q. He
College of Chemical and Biological Engineering
Zhejiang University
Hangzhou, Zhejiang 310027, China
E-mail: qghe@zju.edu.cn
[b] Dr. H. A. Miller, Dr. F. Bartoli, Dr. F. Vizza
Institute of Chemistry of Organometallic Compounds
ICCOM-CNR
Polo Scientifico Area CNR, 50019 Sesto Fiorentino, Italy
E-mail: hamish.miller@iccom.cnr.it
[c] Dr. I. Salam, Prof. J. R. Varcoe
Department of Chemistry
University of Surrey
Guildford, Surrey GU2 7XH, UK
[d] Dr. L. Wu
School of Chemistry and Chemical Engineering and Key Laboratory of Scientific and Engineering Computing of Ministry of Education
Shanghai Jiao Tong University
Shanghai, China
E-mail: liang.wu@sjtu.edu.cn
[e] Dr. Y. Chen, Prof. H. Liao
State Key Laboratory of Physical Chemistry of Solid Surfaces, College of Chemistry and Chemical Engineering
Xiamen University
Xiamen 361005, PR China
[f] Dr. E. Liu, Dr. Q. Jia
Department of Chemistry and Chemical Biology
Northeastern University Center for Renewable Energy Technology
Boston, MA 02115, USA
[g] Dr. Q. He
Ningbo Research Institute
Zhejiang University
Ningbo, Zhejiang 315100, China

Supporting information for this article is given via a link at the end of the document.

Abstract: In anion exchange membrane fuel cells, catalytic reactions occur at a well-defined three-phase interface, wherein conventional heterogeneous catalyst layer structures exacerbate problems such as low catalyst utilization and limited mass transfer. We developed a structural engineering strategy to immobilize a molecular catalyst tetrakis(4-methoxyphenyl)porphyrin cobalt(II) (TMPPCo) on the side chains of an ionomer (polyfluorene, PF) to obtain a composite material (PF-TMPPCo), thereby achieving a homogeneous catalysis environment inside ion flow channels, with greatly improved mass transfer and turnover frequency due to 100% utilization of the catalyst molecules. The unique brand-new structure of the homogeneous catalysis system comprising interconnected nanoreactors exhibits advantages of low overpotential and high fuel cell power density. This strategy of reshaping of the catalyst layer structure may serve as a new platform for applications of many molecular catalysts in fuel cells.

As an emerging technique and attractive potential alternative to the current proton exchange membrane fuel cells, anion exchange membrane fuel cells (AEMFC) are cost effective due to the possible use of non-precious catalyst materials and fuel flexibility.[1]. As the "heart" of AEMFCs, the membrane electrode assembly (MEA) is mainly composed of a gas diffusion layer, a catalytic layer and a polyelectrolyte membrane. Among them, the catalyst layer, where the catalytic reaction takes place, plays a vital role in MEA performance.

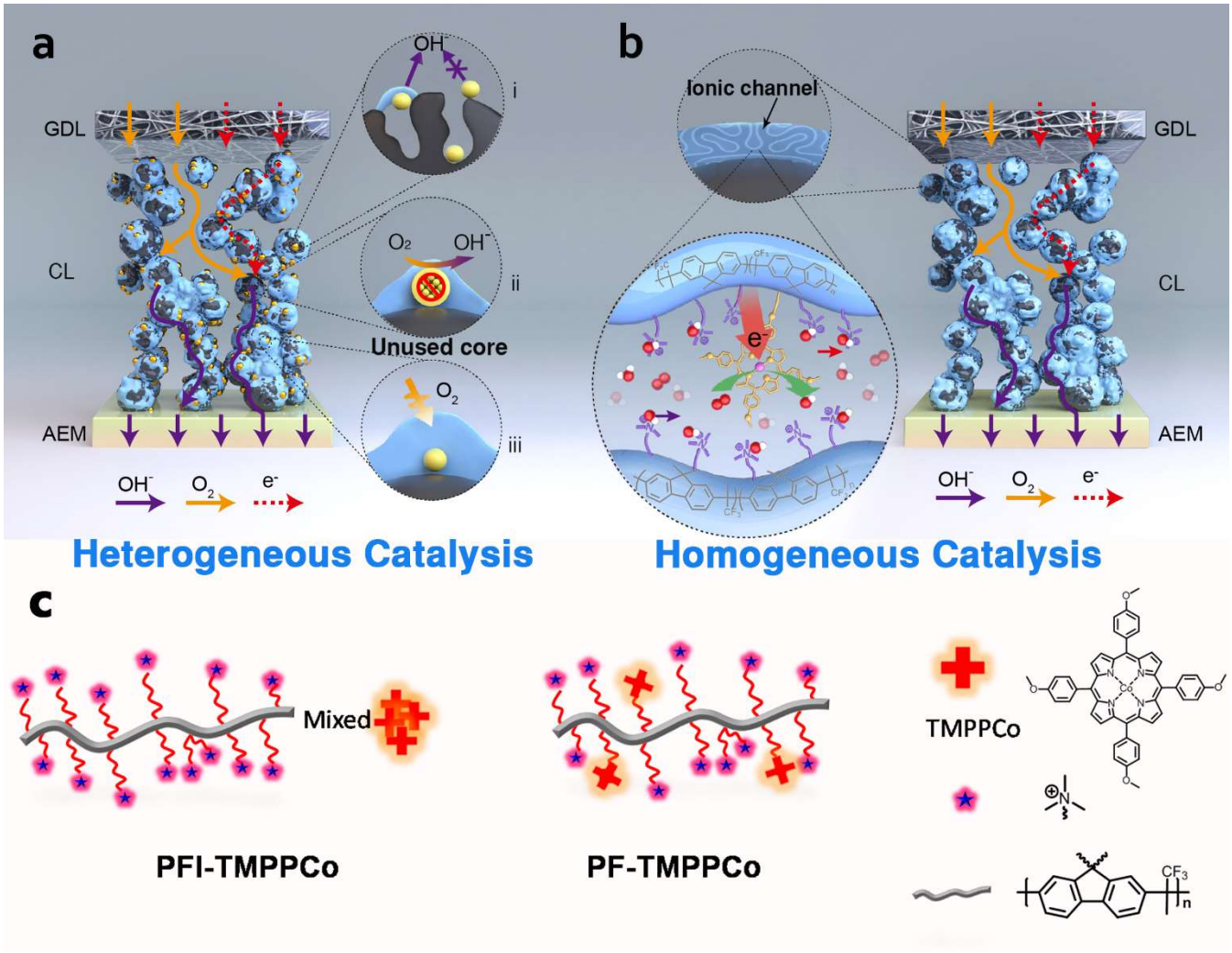

Figure 1. The advantage of the fuel cell catalyst layer based on homogeneous catalysis. a, Conventional catalyst layer based on heterogeneous catalysis: (i) catalyst nanoparticles without covering of the ionomer; (ii) the useful outer shell and unused inner atoms of catalyst nanoparticles; (iii) thick coverage of ionomer on catalyst nanoparticles. b, Catalyst layer based on homogeneous catalysis with TMPPCo molecular catalyst, chemically tethered on side chains of PF ionomers. c, Schematic illustration of PFI-TMPPCo and PF-TMPPCo.

As shown in Figure 1a, the catalyst layer contains nano-catalysts such as Pt/C to complete the catalytic reaction, as well as an ionomer (a type of polymer electrolyte) with a structure similar to that of the ion-exchange membrane. Ionomers act both as binder and ion conductor, thereby constructing a spatial site where the ion conductive material, the electronic conductive material, and the reactant are confined to the catalytic site together, thus allowing the catalytic reaction to occur [2]. Under ideal conditions, the Pt surface will be evenly covered by the ionomer thin film. However, in practical cases, irrespective of the uniform stirring of the ink, a considerable portion of the Pt particles may not be covered by the ionomer during the formation of the catalyst layer; thus, there is no ion conductive pathway, resulting in low catalyst utilization. In order to improve the ion conduction of the catalyst surface, Ralbag et al. used ionomers to dope silver metal catalysts at the molecular level to obtain composite materials with both electrocatalytic and ionic properties[3]. In addition, ionomer crosslinking immobilization[4], nanodispersed ionomer[5] or ionic liquid modification[6] were employed to improve the microenvironment of Pt catalysts to prepare high-performance alkaline membrane fuel cell catalyst layers.

On the other hand, agglomeration or excessive coverage of the ionomer will also hinder the gas diffusion, thereby affecting the catalytic efficiency [7]. In addition, even for the catalyst nanoparticles that can be uniformly covered by an ionomer, because electrocatalysis is a surface interface reaction, the inner atoms of the nanoparticles cannot be used effectively. For example, for a 3.9 nm spherical nano-Pt particle, the proportion of the outermost atoms that can play a catalytic role is only 26% [8]. Therefore, it can be seen that the current catalytic layer structure based on heterogeneous catalysis has several deep-rooted drawbacks: (i) the limitation of the three-phase interface, i.e. Pt nanoparticles that are not covered by ionomers or located in the tiny pores of the support carbon cannot complete the catalytic reaction, (ii) ionomer agglomeration causes resistance to oxygen mass transfer, and (iii) the atoms in the core region of the nanoparticles cannot be used effectively.

These issues prompted us to retrospect the features and advantages of homogeneous catalysis [9]. In homogeneous catalysis, the catalyst exists in the same media as the reaction substance in the molecular state; therefore, the homogeneous catalyst has a high utilization rate, avoids the mass transfer problem of the heterogeneous catalyst, and has better catalytic

selectivity. However, although molecular catalysts are immobilized on the surface of carbon supports or gas diffusion electrodes [10], there are few reports on achieving homogeneous catalytic systems in fuel cells (FC). The difficulty of achieving homogeneous catalysis in the FC catalyst layer lies in how to embed the molecular catalysts evenly and stably in the medium where the oxygen, ion, and electron arrive simultaneously [11]. In the ionomer film of the catalyst layer, there is phase separation through hydrophilic-hydrophobic interactions, in which the hydrophilic part of ionic groups constitute ionic nanochannels, regarded as a homogeneous system from a local perspective [12]. Therefore, to apply the concept of homogeneous catalysis to the FC catalyst layer, the molecular catalyst must be placed in the ion flow channel where the electroactive substance is located.

Thus, in this work, a well-known oxygen reduction reaction (ORR) molecular catalyst 5,10,15,20-[tetrakis(4-methoxyphenyl)porphyrin] cobalt(II) (TMPPCo) was bonded to the side chain of polyfluorene (PF, a high-performance anion exchange ionomer) to form a composite material (PF-TMPPCo). PF is composed of main chains of hydrophobic polyaromatic hydrocarbons and side chains of hydrophilic quaternary ammonium salts, which can induce microphase separation. The TMPPCo molecular catalyst is distributed on the side chain, so the obtained catalyst complex possesses a high density of active sites, which randomly dispersed in ionic conductive media. This covalent immobilization strategy can provide the possibility to build a novel stable homogeneous catalytic system, like interconnected nanoreactors. Most importantly, each catalyst molecule anchored in ionic channels can be used as the active center site of the "three-phase interface", and be theoretically 100 % utilized. TMPPCo moieties that are covalently integrated into the PF ionomer are characterized by ^{1}H NMR, FT-IR, X-ray photoelectron spectroscopy (XPS), X-ray absorption spectroscopy (XAS), etc. After mixing with the carbon carrier, the ORR electrochemical properties and AEMFC performance were investigated.

Figure 1b is a schematic diagram of the homogeneous cathodic molecular catalyst layer based on PF-TMPPCo. Compared with Figure 1a, it can be found that if molecular catalysts are evenly distributed over the ionomer as active sites, all active sites are utilizable theoretically. The experimental procedure used for building the homogeneous catalyst layer are shown in Scheme S1 in the supporting information. First, tetramethoxyphenylporphyrin (TMPP) and 5-phenol-10,15,20-tris(4-methoxyphenyl)porphyrin (TMPP-OH) were prepared by reacting 4-methoxybenzaldehyde or benzaldehyde with pyrrole in propionic acid and confirmed by ^{1}H NMR (Figure S1-S2). Bromoalkyl polyfluorene (PFBr) (Figure S3) was prepared as previously described, by the polymerization of dibromohexyl fluorene and trifluoroacetone under the catalytic conditions of trifluoromethanesulfonic acid, with an average molecular weight of about 47k [13]. Subsequently, TMPP-OH reacted with the bromoalkyl side chain of PFBr and coordinated with cobalt acetate. Therefore, a molecular catalyst active center was successfully introduced to the side chain of PFBr. In order to obtain a hydroxide-conducting ionomer around the molecular catalyst active center, the remaining bromoalkyl groups were quaternized with trimethylamine to obtain PF-TMPPCo, characterized by a PF ionomer containing TMPPCo molecular catalyst groups bound to the side chain. For catalyst layer preparation, an ink composed of PF-TMPPCo, carbon support, and isopropanol was sprayed onto a gas diffusion layer (GDL) after ultrasonic treatment.

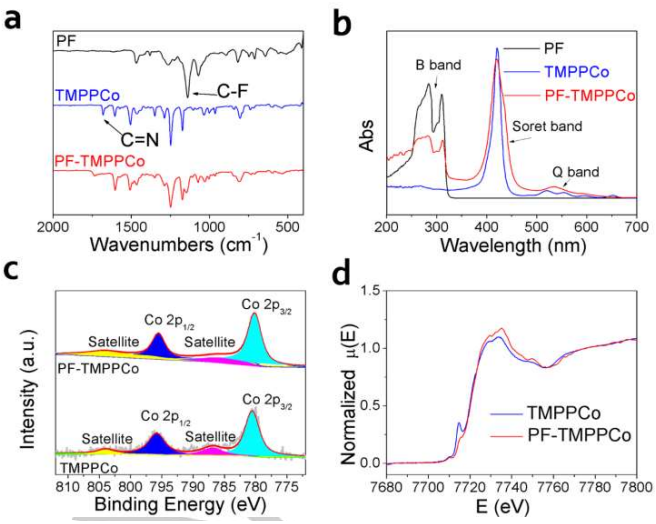

Figure 2. Characterization of the catalyst structure. a, FT-IR and b, UV-vis spectra of PF, TMPPCo, and PF-TMPPCo, c, high-resolution XPS Co 2p spectra for TMPPCo and PF-TMPPCo, d, Co K-edge of TMPPCo and PF-TMPPCo in XANES spectra.

To confirm the successful preparation of PF-TMPPCo, both the FT-IR and UV-vis spectra of PF-TMPPCo were compared to the PF ionomer and molecular catalyst TMPPCo (Figure 2). In IR spectroscopy, as shown in Figure 2a, the characteristic C-F peak of PF at 1042 cm^{-1} and C = N peak of TMPPCo at 1677 nm^{-1} were displayed in PF-TMPPCo. In Figure 2b, the UV-vis absorption spectrum of TMPPCo showed a Soret band at 419 nm and Q band at 529 nm and 613 nm [14], while the absorption of PF at around 250-320 nm can be attributed to the aromatic B band. In PF-TMPPCo, both the aromatic B band of the polymer backbone and the Soret band of TMPPCo had a good correspondence. These results support the successful covalent attachment of TMPPCo on PF by ether bonding.

The survey spectra of the XPS in Figure S4 revealed the existence of all elements of Co, N, C, O, and F. In the high-resolution Co 2p XPS spectrum (Figure 2c), the binding energy peaks located at 781.1 eV and 797.0 eV correspond to the spin orbitals of Co $2p_{3/2}$ and $2p_{1/2}$ assigned to Co-N_4. Typically, pronounced satellite peaks at 787 eV and 804 eV may be attributed to the shakeup excitation of the high-spin Co^{2+} states [15]. Nevertheless, there was only negligible satellite peak, which indicates that TMPPCo molecules were evenly and isolatedly tethered on the side chain of PF [16] and no agglomeration of TMPPCo clusters formed.

The chemical state and coordination environment of Co were further investigated by XAS. As displayed in the X-ray absorption near-edge structure (XANES) spectra (Figure 2d), the absorption edge of Co in PF-TMPPCo was consistent with that of TMPPCo, indicating a similar valence state and coordinated configuration of Co-N_4 in these two catalysts. However, one could note that the intensity of the pre-edge peak is different before and after TMPPCo was attached to the PF. This pre-edge peak may result from the distortion-induced 1s to 3d transition in a six-fold-coordinated cation system and the disturbed symmetry of the M-N_4 (M represents the transition metal) structure [17]. Thus, we believe that the weakness of the

pre-edge peak of PF-TMPPCo may be attributed to the covalent bonding with PF.

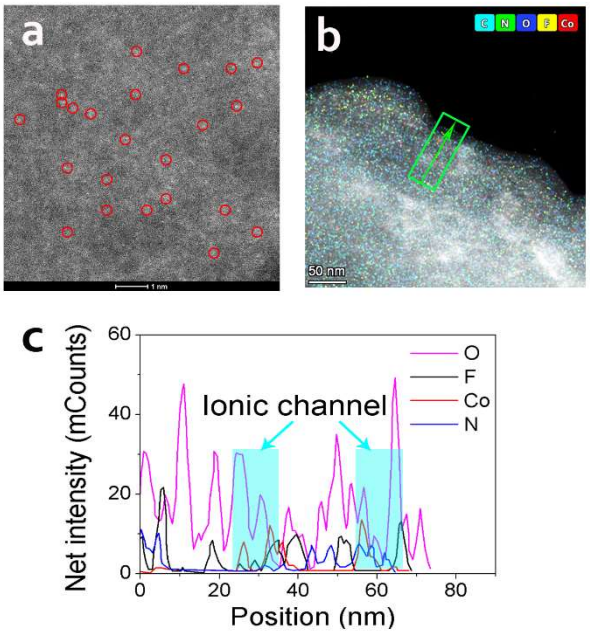

Figure 3. Micromorphology of the catalyst. a, Atomic-resolution high-angle annular dark-field scanning transmission electron microscopy (HAADF-STEM) image of PF-TMPPCo (single Co atoms showing bright contrast). b, Energy-dispersive X-ray spectroscopy images of PF-TMPPCo. c, Net-scanning intensity profile from the area indicated with a green rectangle in Figure 3b, the light blue rectangle corresponds to the ionic channel region.

The micromorphology of the carbon supported PF-TMPPCo was investigated by scanning electron microscopy (SEM) and transmission electron microscopy (TEM). Only the ionomer bound aggregated carbon particles could be observed due to the limitation of SEM magnification (Figure S5a and Figure S5b). Therefore, the precise microscopic morphology of the catalyst was observed by high-resolution TEM. As shown in Figure 3a, isolated white dots were observed for PF-TMPPCo, suggesting the presence of molecular catalyst TMPPCo sites. The energy-dispersive X-ray spectroscopy images (Figure 3b and Figure S5c) and the line-scanning intensity profile (Figure 3c) revealed that Co was distributed at the position containing N and O. In contrast, Co atoms were far away from the F atoms of the hydrophobic main chains. Given the fact that there is a phase separation between the hydrophobic polymer main chain and the hydrophilic side chain, these observations indicate that TMPPCo is well distributed in the ionic channels of the hydrophilic domains. In the mixture of TMPPCo and PF ionomer (PFI-TMPPCo), TMPPCo mainly existed as clusters in the composite (Figure S5d), which proved that immobilization promotes the uniform distribution of the molecular catalyst TMPPCo in the ionomer. This uniform distribution of porphyrin rings in PF-TMPPCo was also observed in the simulation results of all-atom molecular dynamics simulations (Figure S6 and Figure S7).

The ORR performance of PF-TMPPCo and the reference samples, including PFBr-TMPPCo (without QA), PF-TMPP (without Co), and PFI-TMPPCo (mixture of PF ionomer and TMPPCo) was characterized by rotating disk electrode (RDE) experiments in an O_2-saturated 0.1 M KOH solution. Relative to the similar CVs under Ar (Figure S8), more prominent differences for polarization curves at 900 rpm are depicted in Figure 4a. Among the electrocatalysts, PF-TMPPCo exhibited the highest ORR catalytic activity with a half-wave potential of 0.81 V *vs.* RHE, which is 40 mV higher than that of PFI-TMPPCo (0.77 V *vs.* RHE), verifying the advantages of a homogeneous catalyst structure, which enables molecular

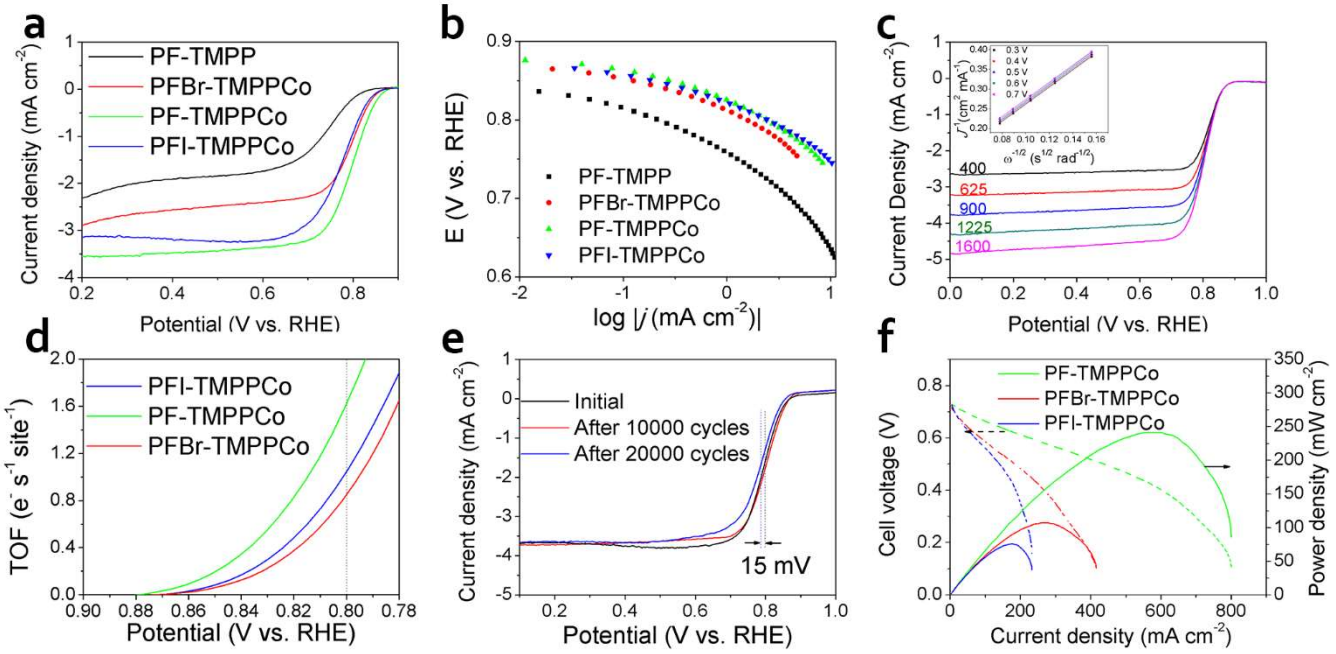

Figure 4. Electrochemical properties of the catalysts. a, ORR polarization curves and b, Tafel curves of different catalysts at a rotating speed of 900 rpm, catalyst loading 0.9 μg_{Co} cm^2. c, ORR polarization curves of PF-TMPPCo at different rotating speeds. The inset is a K-L plot of the current density reciprocal (j^{-1}) vs. $\omega^{-1/2}$ at different potentials. d, TOF of the Co site in PF-TMPPCo, PFI-TMPPCo, and PFBr-TMPPCo. e, Stability test: LSV curves of PF-TMPPCo before and after different potential cycles. f, H_2/O_2 AEMFC test. Anode: PtRu/C. Membrane: HDPE-VB-TMA. The graphs indicate power density (solid lines), and cell voltage V (dotted lines) vs. current density.

catalysis and a uniform dispersion of three-phase interfaces. Moreover, the ORR activity of PF-TMPP is inferior to that of PF-TMPPCo, indicating that the Co center serves as the active site in the ORR process. Moreover, PFBr-TMPPCo also exhibited a lower half-wave potential (0.79 V *vs.* RHE) than PF-TMPPCo, which is attributed to the absence of quaternary ammonium and potential Br^- poisoning caused by hydrolysis[18]. This reveals the importance of ion channels, efficient mass transfer of H_2O, O_2, and OH^-, and the formation of a three-phase interface in ORR catalysis.

To obtain more information regarding the ORR kinetics and mechanisms, Tafel plots for the above catalysts were constructed as shown in Figure 4b and Figure S9. From Figure S9 and Table S1, the Tafel slopes of PFI-TMPPCo, PFBr-TMPPCo, and PF-TMPPCo are 57, 55, and 67 mV/dec, respectively, in the low overpotential region. The slope values approaching 60 mV/dec indicate a similar reaction pathway and the same rate-determining step as Co-based macrocycles in alkaline media[19]. At higher overpotential regions, all three samples exhibited Tafel slopes slightly larger than 120 mV/dec, implying the Co^I state becomes gradually predominant in the rate-determined step[19]. For the PF-TMPP catalyst without Co metal center, although with relatively poor kinetic performance，a Tafel slope of 62 mV/dec indicates that the second electron transfer, consisting of the $O_2H_{,ads}$ species electrosplitting and yielding O_{ads} and hydroxide anion is rate determining[20]. A Tafel slope of 184 mV/dec (rather than standard 120 mV/dec) at lower potentials for PF-TMPP is attributed to electrode properties arising from factors such as non-uniformity of pore distribution, thickness, or conductivity from carbon materials[21].

Furthermore, polarization curves recorded at various rotation speeds and Koutecky–Levich (K–L) plots for PF-TMPPCo in Figure 4c provide insights on the reaction pathways. The value of the electron-transfer number (Eq. S1) derived from the K–L plots for PF-TMPPCo reached 4.1, suggesting complete oxygen reduction to H_2O. By contrast, PFBr-TMPPCo and PFI-TMPPCo displayed exchange-electron numbers of 2.97 and 3.32 (Table S1 and Figure S10), respectively, implying a mixture of 2-electron and 4-electron pathways, which is consistent with the reported electron number for the Co-based macrocycle catalyst[22]. This indicates that the homogeneous catalyst structure helps to boost the 4-electron transfer pathway. From Figure S10 and Table S1, a near 2-electron pathway was observed for PF-TMPP without Co active centers, demonstrating the incomplete reduction of oxygen to hyperoxide.

The turnover frequencies (TOFs) of the Co sites in the catalysts were the number of electrons reduced per active site per second, which can be calculated from the kinetic current and mass-based Co site densities according to Eq. S2 in the Supporting Information [23]. From Figure 4d, the TOF of the Co site in PF-TMPPCo is 1.63 $e^- s^{-1}$ $site^{-1}$ at 0.8 V, nearly twice that of PFBr-TMPPCo (0.81 $e^- s^{-1}$ $site^{-1}$) and 1.6 times that of PFI-TMPPCo (1.03 $e^- s^{-1}$ $site^{-1}$). This result could be due to two possibilities: (i) an improved intrinsic catalytic activity of a single site in PF-TMPPCo and (ii) an increased number of utilized active sites in PF-TMPPCo.

Moreover, the stability of PF-TMPPCo was demonstrated by 10000 continuous cycles ranging from 0.6 to 1.0 V vs. RHE at a scan rate of 100 mV s^{-1} in an O_2-saturated 0.1 M KOH solution. At the end of the cycling, PF-TMPPCo presented a negligible loss of linear sweep voltammetry (LSV) curves with the initial cycle (Figure 4e). More extreme tests show that even after 20,000 cycles, there was only a loss of 15 mV for $E_{1/2}$ and no significant change in CVs before and after stability test (Figure S11), highlighting the excellent ORR stability. While for PFI-TMPPCo, there was an attenuation of nearly 20 mV after 5000 cycles (Figure S12). This comparison proves that the stability of PF-TMPPCo comes from covalent bonding structure.

The three catalysts; PF-TMPPCo, PFBr-TMPPCo and PFI-TMPPCo were also tested in fuel cells together with a high performance AEM and a commercial PtRu/C material as hydrogen oxidation anode catalyst. The membrane used for the fuel cell tests was high-density polyethylene (HDPE) vinyl benzyl trimethylammonium (HDPE-VB-TMA), the properties of which can be seen in Table S2 [24]. In Figure 4f, we report the fuel cell performance of the three cathode catalysts. PF-TMPPCo exhibited the best performance, where the peak power density was 226 mW/cm^2 at a current density of 509 mA/cm^2. The other two catalysts achieved 97 mW/cm^2 (PFBr-TMPPCo) and 58 mW/cm^2 (PFI-TMPPCo) respectively. The difference in performance can be justified as follows. There is no QA group located near the catalytic center of PFBr-TMPPCo, which significantly slows down ORR kinetics, reduces catalyst utilization, and weakens the ionic conductivity of the catalyst layer. While for PFI-TMPPCo, even with the same metal loading, due to the aggregation of the molecular catalyst and the non-uniform blending of ionomer and catalyst, the effective active sites in the catalyst layer were greatly reduced, so that it exhibited the lowest AEMFC performance. The PF-TMPPCo cathode with aligned catalyst sites in ion conducting channels has optimized performance. This is also shown by the very low area specific resistance (ASR, see Table S2) of the MEA during fuel cell testing, showing less ohmic losses due to improved ionic conduction. From Table S2 and Table S3, the improved performance of PF-TMPPCo in fuel cell tests becomes more obvious than the RDE testing, which is due to the thicker catalyst layer in the fuel cell and the higher mass transfer requirements.

In conclusion, TMPPCo was immobilized on the side chain of the PF ionomer and distributed within the ionic channels to obtain a homogeneous catalytic system in the AEMFC catalyst layer. In this structure, the molecular catalysts coexist with the reactants and the reaction products in the medium located in the ion channels, which greatly enhances the catalyst utilization rate and improves the mass transfer. The appearance of characteristic peaks in NMR, FT-IR, and UV-vis spectra indicated that TMPPCo was successfully grafted onto the PF side chain. HR-TEM and molecular dynamics simulations showed that due to the phase separation of polyelectrolytes, molecular catalysts were uniformly distributed in the ionic channels that were formed by the local arrangement of quaternary ammonium groups and served as anion conductive pathways.

The thus obtained PF-TMPPCo shows excellent ORR activity with $E_{1/2}$=0.81 V and durability tests showed that the LSV was nearly unchanged after 10,000 cycles, indicating the remarkable electrochemical stability. The homogeneous system also results in high utilization of active sites, with a TOF three times that of the PFI-TMPPCo (mixture of PF ionomer and TMPPCo). More importantly, the peak power density of an AEMFC using the cathode catalyst layer composed of PF-TMPPCo was twice that of PFBr-TMPPCo (without QA group) and nearly four times that

of physical mixture of PFI-TMPPCo, indicating the improved mass transfer of oxygen, water and hydroxide, electrochemical kinetic activity, and utilization of catalyst active sites in the catalyst layer based on homogeneous catalysis. This design strategy of reshaping catalyst layer may also be extended to other electrochemical energy conversion devices to fulfill the real application of non-noble metal materials by simply improving mass transfer and catalytic site utilization.

Acknowledgements

Q.H. acknowledges the financial support from the National Natural Science Foundation of China (Grant Nos. 21676241, U1732111 and 21978260). The collaboration between ICCOM (CNR) teams and the University of Surrey was facilitated by funding from the Royal Society's International Exchange Scheme (Grant No. IES\R3\170134). We also thank Ente Cassa di Risparmio Di Firenze for funding (Project EnergyLab) and the PRIN 2017 Project funded by the Italian Ministry of MIUR Italy (Grant No. 2017YH9MRK). L.W. acknowledges young researcher start-up fund from Shanghai Jiao Tong University.

Conflict of interest

The authors declare no conflict of interest.

Keywords: homogeneous catalysis • oxygen reduction reaction • anion exchange membrane fuel cell • cathodic catalyst layer

[1] a) E. S. Davydova, S. Mukerjee, F. Jaouen, D. R. Dekel, *ACS catal.* **2018**, *8*, 6665-6690; b) S. Zhao, L. Yan, H. Luo, W. Mustain, H. Xu, *Nano Energy* **2018**, *47*, 172-198; c) V. Vijayakumar, S. Y. Nam, *J. Ind. Eng. Chem.* **2019**, *70*, 70-86; d) Q. He, E. J. Cairns, *J. Electrochem. Soc.* **2015**, *162*, 1504-1539.

[2] a) A. Katzenberg, A. Chowdhury, M. Fang, A. Z. Weber, Y. Okamoto, A. Kusoglu, M. A. Modestino, *J. Am. Chem. Soc.* **2020**, *142*, 3742-3752; b) S. Maurya, S. Noh, I. Matanovic, E. J. Park, C. Narvaez Villarrubia, U. Martinez, J. Han, C. Bae, Y. S. Kim, *Energy Environ. Sci.* **2018**, *11*, 3283-3291.

[3] N. Ralbag, M. Mann-Lahav, E. S. Davydova, U. Ash, R. Galed, M. Handl, R. Hiesgen, E. Magliocca, W. Mustain, J. He, P. Cong, A. M. Beale, G. S. Grader, D. Avnir, D. R. Dekel, *Matter* **2019**, *1*, 959-975.

[4] a) X. Liang, M. A. Shehzad, Y. Zhu, L. Wang, X. Ge, J. Zhang, Z. Yang, L. Wu, J. R. Varcoe, T. Xu, *Chem. Mater.* **2019**, *31*, 7812-7820; b) D. Dru, S. Baranton, J. Bigarré, P. Buvat, C. Coutanceau, *ACS catal.* **2016**, *6*, 6993-7001.

[5] C.-Y. Ahn, J. Ahn, S. Y. Kang, O.-H. Kim, D. W. Lee, J. H. Lee, J. G. Shim, C. H. Lee, Y.-H. Cho, Y.-E. Sung, *Science Advances* **2020**, *6*, eaaw0870.

[6] G.-R. Zhang, T. Wolker, D. J. S. Sandbeck, M. Munoz, K. J. J. Mayrhofer, S. Cherevko, B. J. M. Etzold, *ACS catal.* **2018**, *8*, 8244-8254.

[7] a) G. Inoue, T. Ohnishi, M. So, K. Park, M. Ono, Y. Tsuge, *J. Power Sources* **2019**, *439*, 227060; b) S. Holdcroft, *Chem. Mater.* **2014**, *26*, 381-393; c) T.-H. Kim, J. H. Yoo, T. Maiyalagan, S.-C. Yi, *Appl. Surf. Sci.* **2019**, *481*, 777-784; d) A. Uddin, L. Dunsmore, H. Zhang, L. Hu, G. Wu, S. Litster, *ACS Appl. Mater. Interfaces* **2020**, *12*, 2216-2224.

[8] L. Zhang, L. T. Roling, X. Wang, M. Vara, M. Chi, J. Liu, S.-I. Choi, J. Park, J. A. Herron, Z. Xie, M. Mavrikakis, Y. Xia, *Science* **2015**, *349*, 412-416.

[9] a) M. L. Pegis, C. F. Wise, D. J. Martin, J. M. Mayer, *Chem. Rev.* **2018**, *118*, 2340-2391; b) Q. He, T. Mugadza, G. Hwang, T. Nyokong, *Int. J. Electrochem. Sci.* **2012**, *7*, 7045-7064.

[10] a) C. Costentin, H. Dridi, J.-M. Savéant, *J. Am. Chem. Soc.* **2015**, *137*, 13535-13544; b) S. Dey, B. Mondal, S. Chatterjee, A. Rana, S. Amanullah, A. Dey, *Nat. Rev. Chem.* **2017**, *1*, 0098.

[11] Q. He, T. Mugadza, X. Kang, X. Zhu, S. Chen, J. Kerr, T. Nyokong, *J. Power Sources* **2012**, *216*, 67-75.

[12] a) K. Schmidt-Rohr, Q. Chen, *Nat. Mater.* **2008**, *7*, 75-83; b) R. Sun, Z. Xia, X. Xu, R. Deng, S. Wang, G. Sun, *Nano Energy* **2020**, 104919.

[13] S. Ren, D. Joulié, D. Salvatore, K. Torbensen, M. Wang, M. Robert, C. P. Berlinguette, *Science* **2019**, *365*, 367-369.

[14] Q. He, G. Wu, K. Liu, S. Khene, Q. Li, T. Mugadza, E. Deunf, T. Nyokong, S. W. Chen, *ChemElectroChem* **2014**, *1*, 1508-1515.

[15] Y. Lian, W. Yang, C. Zhang, H. Sun, Z. Deng, W. Xu, L. Song, Z. Ouyang, Z. Wang, J. Guo, Y. Peng, *Angew. Chem. Int. Ed.* **2020**, *59*, 286-294.

[16] S. Roy, E. Reisner, *Angew. Chem. Int. Ed.* **2019**, *58*, 12180-12184.

[17] Z. Wu, D. C. Xian, C. R. Natoli, A. Marcelli, E. Paris, A. Mottana, *Appl. Phys. Lett.* **2001**, *79*, 1918-1920.

[18] P. G. Santori, A. N. Mondal, D. R. Dekel, F. Jaouen, *Sustainable Energy & Fuels* **2020**, *4*, 3300-3307.

[19] J. H. Zagal, M. T. M. Koper, *Angew. Chem. Int. Ed.* **2016**, *55*, 14510-14521.

[20] I. Roche, E. Chaînet, M. Chatenet, J. Vondrák, *The Journal of Physical Chemistry C* **2007**, *111*, 1434-1443.

[21] a) K. I. Ozoemena, S. A. Mamuru, T. Fukuda, N. Kobayashi, T. Nyokong, *Electrochemistry Communications* **2009**, *11*, 1221-1225; b) J. N. Soderberg, A. C. Co, A. H. C. Sirk, V. I. Birss, *The Journal of Physical Chemistry B* **2006**, *110*, 10401-10410.

[22] C. W. Machan, *ACS catal.* **2020**, *10*, 2640-2655.

[23] J.-C. Li, S. Maurya, Y. S. Kim, T. Li, L. Wang, Q. Shi, D. Liu, S. Feng, Y. Lin, M. Shao, *ACS catal.* **2020**, *10*, 2452-2458.

[24] L. Wang, J. J. Brink, Y. Liu, A. M. Herring, J. Ponce-González, D. K. Whelligan, J. R. Varcoe, *Energy Environ. Sci.* **2017**, *10*, 2154-2167.

10.1002/anie.202012547

Entry for the Table of Contents

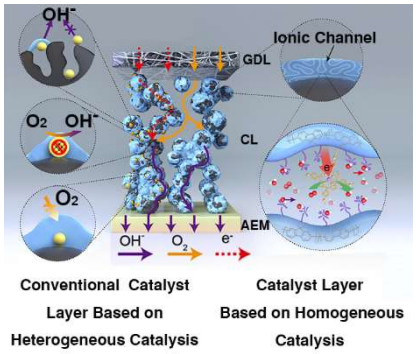

Different from the traditional design, a molecular catalyst (TMPPCo) was anchored on the side chain of a polyfluorene ionomer to establish a homogeneous catalytic system, where the catalysts exist in the same ion flow channels with the reaction substances. With interconnected nanoreactors throughout the catalyst layer, electrochemical kinetic activity, mass transfer, utilization of catalyst active sites and the fuel cell performance were significantly improved.